Tunable Magnetic and Electrical Properties of Cobalt and Zinc Ferrites $CO_{1-X}Zn_XFe_2O_4$ Synthesized by Combustion Route

Saulo Gregory Carneiro Fonseca[a], Laédna Souto Neiva[b], Maria Aparecida Ribeiro Bonifácio[c]*,

Paulo Roberto Cunha dos Santos[a], Ubiratan Correia Silva[d], João Bosco Lucena de Oliveira[a]

[a]*Programa de Pós-Graduação em Química, Instituto de Química, Universidade Federal do Rio Grande do Norte, Natal, RN, Brasil*
[b]*Departamento de Engenharia de Materiais, Universidade Federal do Cariri, Juazeiro do Norte, CE, Brasil*
[c]*Departamento de Engenharia de Materiais, Universidade Federal de Campina Grande, Campina Grande, PB, Brasil*
[d]*Departamento de Física Teórica e Experimental, Universidade Federal do Rio Grande do Norte, Natal, RN, Brasil*

Co and Zn ferrites with general formula $CO_{1-X}Zn_XFe_2O_4$ (x = 0; 0,2 and 0,8) were synthesized by combustion reaction method, using urea as fuel. The structure of inverse-spinel-type ferrite were characterized through XRD using Rietveld refinement method to identify, quantify phases and determine lattice parameters. The crystallites had mean size of 37,33 nm, 43,66 nm and 51.88 nm with the increment of Zn^{2+}, respectively. Samples were sintered in a resistive oven at 900 °C for 3 hours. Analysis by SEM indicated that the particles have irregular sizes and high concentration of open pores. The magnetic properties were measured using a vibrating sample magnetometer (VSM), through which a decrease in the magnetization variation was observed as the non-magnetic Zn^{2+} concentration increases. The permittivity and loss tangent were determined using vector network analyzer equipment, permittivity increases with the increase of zinc concentration and the tangent loss measurements were small for all ferrites synthesized in this work.

Keywords: *cobalt and zinc ferrites, combustion synthesis, magnetic properties, electrical properties.*

1. Introduction

Spinel ferrites such as zinc ferrites, have great potential for applications in multi-functional devices such as magnetic field sensors, memory devices[1,2], electric field converters in microwave region, electromagnetic wave filters, phase shifters, waveguides, oscillators and others[3]. Nanopowders of ferrites exhibits special magnetics and electrical properties, that are sensible to structure, synthesis method, particle size and cation distribution between A and B sites[4]. Ferrites have a general formula AB_2O_4, in which A has tetrahedral sites and B has octahedral sites, its well known that ferrites can be assumed an inverse format spinel, wherein the B site atoms can migrate to the positions of A site atoms, and the A site atoms can migrate to the positions of B site, this property of cation migration between sites is responsible for the tunable technical features of ferrites[5].

The search for ceramic nanostructured materials with important physical and chemical properties has been the major focus of intensive research by several groups around the world[6,7], ferrites were synthesized by various routes such as ceramic[8], Sol-Gel[9], hydrothermal[10], Pechini route[11], and others. In this context, combustion method has been used to obtain ferrite based materials of various metals, combustion is characterized by producing pure powders at low cost and with a short time of synthesis. Some works related that this method can obtain nanopowders with high crystallinity[12]. In combustion method the choice of a suitable reducer has an important hole. Among the most commonly used reducers are urea, glycine and carbohydrazin. All mentioned reducers act as fuels. The heat released by the fuel should be enough for the formation of desired products. Several works reported that urea is a fuel used to form nanopowders and, during the reaction, a large amount of gases are formed, which favors powders with high crystallinity and homogeneity[13-15].

$CoFe_2O_4$ is a well known hard magnetic ferrite, with moderate saturation magnetization and high coercive field, that can be modified by addition of amounts of Zn^{2+}. In our research we admit that Zn^{2+} can migrate to tetrahedral and octahedral positions. This continuous migration modifies the magnetic and electrical properties[16]. In this paper we relate that the substitution of Co^{2+} by Zn^{2+} causes a decrease in lattice parameter and an abruptly change in anisotropy constant with formation of superparamagnetic material.

In the present work, cobalt and zinc ferrites with composition $Co_{(1-X)}Zn_{(X)}Fe_2O_4$ (where X = 0,0; 0,2 and 0,8) were synthesized. X-Ray Powder Diffraction (XRD), Rietveld method, Scanning Electron Microscopy (SEM), vibrating sample magnetometer (VSM) and electrical properties, such as permittivity and loss tangent, were measured at room temperature, with the objective to determine the influence of Zn^{2+} addition on the structural parameters, magnetic properties and a cation distribution between A and B sites of ferrites.

2. Material and Methods

2.1 Chemicals and synthesis

All chemicals $Co(NO_3)_2.6H_2O$, $Zn(NO_3)_2 \cdot 6H_2O$, $Fe(NO_3)_3 \cdot 9H_2O$, $[CO(NH_2)_2]$, were purchased from Sigma-Aldrich, with purity > 98 %. The combustion method reactions for obtaining ceramic powders was used to synthesize powders. The salts $Co(NO_3)_2.6H_2O$; $Zn(NO_3)_2.6H_2O$, and $Fe(NO_3)_3.9H_2O$, were used as precursor reagents (oxidants) and as source of cations. Urea was used as fuel and reducing agent $CO(NH_2)_2$, all weighed, mixed, solubilized and homogenized in 10 mL of deionized water. Stoichiometry, mass ratio and number of moles of each component were determined based on the chemistry of propellants and explosives, which are based on the total valence of oxidants and reductants reagents. In combustion method, the valence of elements are used in form to establish a relation between quantities of oxidants and fuels (reductants), with basis in stoichiometry established previously. In propellant chemistry was defined the concepts of valences of oxidizing and reductants[17-18], carbon, hydrogen, iron, cobalt, and zinc, with respective valences +4, +1, +3 and +2, oxygen is considered like as oxidant element with valence -2, and nitrogen is a neutral element with valence equal a 0. The valences for all species are $Fe(NO_3)_3.9H_2O$ = -15, $Co(NO_3)_2.6H_2O$ = -10, $Zn(NO_3)_2.6H_2O$ = -10, $CO(NH_2)_2$ = +6, the quantity of $CO(NH_2)_2$ which will be used in combustions reactions is determined by equation 1:

$$\Sigma \, Oxidants \, Valences + Reduc\tan ts \, Valences = 0 \quad (1)$$

For ferrites with general formula $CO_{1-X}Zn_XFe_2O_4$, the amount of Urea is calculated by -10 .(Quantity in A site)+(-15) .(Quantity in B site)+6.n=0, thequantity of urea is n = 6,67, for balancing we will consider the value 7. When valences are balanced, we can get the stoichiometry admitting that some gases are formed in reactions of combustions such as, $CO_{2(g)}$, $NO_{2(g)}$, $H_2O(g)$. The combustion reactions involved in the synthesis of all samples are described below:

$$Co(NO_3)_2 \cdot 6H_2O_{(S)} + 2Fe(NO_3)_3 \cdot 9H_2O_{(S)} +$$
$$7CO(NH_2)_{2(S)} + \frac{3}{2}O_{2(g)} \rightarrow CoFe_2O_{4(S)} +$$
$$11N_{2(g)} + 38H_2O_{(g)} + 7CO_{2(g)} \, 0,8Co(NO_3)_2 \cdot$$
$$6H_2O_{(S)} + 0,2Zn(NO_3)_2 \cdot 6H_2O_{(S)} +$$
$$2Fe(NO_3)_3 \cdot 9H_2O_{(S)} + 7CO(NH_2)_{2(S)} + \frac{3}{2}O_{2(g)} \rightarrow$$
$$Co_{0,8}Zn_{0,2}Fe_2O_{4(S)} + 11N_{2(g)} + 38H_2O_{(g)} + 7CO_{2(g)}$$
$$0,2Co(NO_3)_2 \cdot 6H_2O_{(S)} + 0,8Zn(NO_3)_2 \cdot 6H_2O_{(S)} +$$
$$2Fe(NO_3)_3 \cdot 9H_2O_{(S)} + 7CO(NH_2)_{2(S)} + \frac{3}{2}O_{2(g)} \rightarrow$$
$$Co_{0,2}Zn_{0,8}Fe_2O_{4(S)} + 11N_{2(g)} + 38H_2O_{(g)} + 7CO_{2(g)}$$
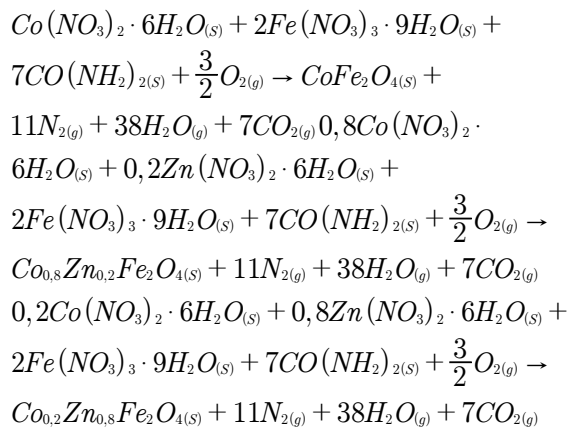
Precursors are placed in a crucible and heated to undergo combustion process. Upon heat in the hot plate and the heat released by urea, the temperature of the reaction medium is progressively increased, then combustion reaction is clear when the high-viscosity mixture reaches temperature around at 450°C. Reaction process is carried out within a few seconds, exceeding temperature of 600°C. Consequently, ceramic powders are obtained.

2.2 Instrumentation

The X-ray diffractograms were made on XRD-7000 from Shimadzu, measurement conditions of the ceramic materials were recorded operating at 40 kV of tension and current of 30 mA. With a scan step of 0.02° and 2θ pre timing defined in 1,2 seconds, in the 2θ range of 15° to 80°. Ferrites obtained by combustion, which are ceramic powders from mixtures of upper nanostructured oxides, were characterized by XRD and then the diffraction data received refinement treatment by the Rietveld method. The methodology application of the Rietveld method used in this study is described in Abhijit et al. (2012)[1]s, Scanning Electron Microscopy (SEM) was performed with TM 3000 from Hitachi, with magnification of 5000x on 15 kV and resolution of 512 x 384 pixels, with images of 32,3 μm for these compositions.

Magnetic characterizations were measured using a vibrating sample magnetometer (VSM) that allows measures in range between 77 - 650 K in magnetic fields until 10 kOe. Electrical properties such as permittivity and loss tangent were determined using a vector network analyzer equipment ROHDE & SCHWARZ model ZVB14.

3. Results and Discussion

3.1 XRD analysis and rietveld method

The XRD patterns of all samples are shown in figure 1 for $CoFe_2O_4$. The observed peaks indicate three phases that can be attributed to the presence of a major phase of spinel COD (Card nº. 1535820, space group Fd-3m), and a minor phase of Fe_2O_3 COD (Card nº. 1546383, space group R - 3c)

Tunable Magnetic and Electrical Properties of Cobalt and Zinc Ferrites CO$_{1-X}$Zn$_X$Fe$_2$O$_4$ Synthesized by Combustion Route

3

and an unknown phase that we cannot index to any card. For $Co_{0,8}Zn_{0,2}Fe_2O_4$ was observed a formation of two phases that can be indexed to major spinel phase COD (Card nº. 9006894, space group Fd-3m) and a minor phase of Fe_2O_3. For $Co_{0,2}Zn_{0,8}Fe_2O_4$ was observed a single-phase with characteristic peaks of spinel, the observed peaks can be indexed to COD (Card nº. 9006894, space group Fd-3m) all the cards used in indexes in XRD also employed in Rietveld refinement.
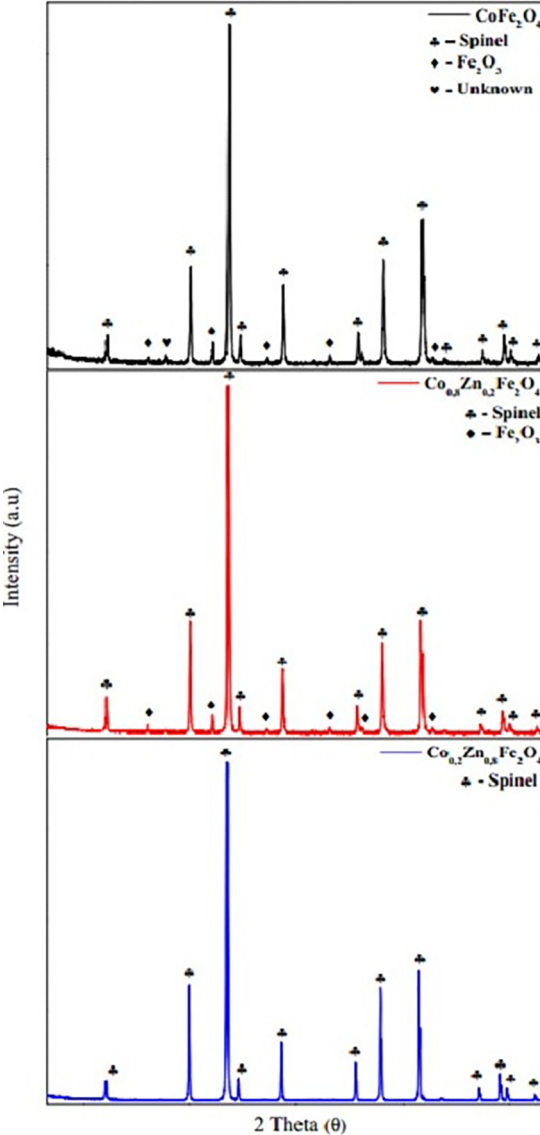
Figure 1. XRD patterns a-) $CoFe_2O_4$, b-) $Co_{0,2}Zn_{0,8}Fe_2O_4$, c-) $Co_{0,8}Zn_{0,2}Fe_2O_4$

The crystallite size of all samples were estimated from the line broadening of the most intense peak in spinel (311), using Scherrer equation 2:

$$D = \frac{K \cdot \lambda}{\beta \cdot \cos\theta} \qquad (2)$$

In Scherrer equation, D corresponds to crystallite size, λ is the wavelength of the incident x-ray, 2θ is the Bragg angle and β is the full width at half maximum (FWHM) of the most intense peak and K is a shape factor equal to 0,94. All results from crystallites sizes and crystallinities are summarized in table 1. The crystallite size and crystallinity increases with concentration of Zn^{2+}.

In figure 1 we observed a continuously shift to small 2θ angles, that indicates an increase in lattice parameter, such shift indicates that this growth in lattice parameter may be justified by the differences between ionic radii of A and B sites. To justify the lattice growth we admit three hypotheses: first of all, atoms of Fe can exist in forms of Fe^{2+} and Fe^{3+}, Fe^{2+} and Fe^{3+} can migrate to octahedral and tetrahedral sites. We also admit Co^{2+} and Zn^{2+} can occupy sites A and B. The lattice constant was calculated by following equations 3 and 4[19-20]:

$$\frac{1}{d_{hkl}^2} = \frac{h^2 + k^2 + l^2}{a^2} \qquad (3)$$

$$n \cdot \lambda = 2 \cdot d \cdot sen\theta \qquad (4)$$

In that equation, "d_{hkl}" is the interplanar spacing, estimated by Bragg equation 4, on which "h k l" are miller indices, and "a" is lattice parameter.

By the possibility about cation migrations between both sites, we can investigate the lattice parameter for $CoFe_2O_4$. For this we need to analyze the cations radii obtained from radii database[21], Co^{2+} (0,58 Å, 0,745 Å) these values are for tetrahedral and octahedral sites, respectively. When Co^{2+} migrates to B site replacing Fe^{3+} (0,49 Å, 0, 645 Å) and Fe^{2+} (0,63 Å, 0,78 Å), the lattice parameter decrease in part because Co^{2+} has a larger radii over Fe^{3+}. By cation distribution in table 4, we observe that the most part in A site is composed by Fe^{3+}, a small cation when compared with Co^{2+}. For this reason we observe shrinkage in a lattice parameter when compared with another ferrites synthesized in this work, substituted by Zn^{2+}. For $Co_{0,8}Zn_{0,2}Fe_2O_4$ the Zn^{2+} (0,6 Å , 0,74 Å) and Co^{2+} replace Fe^{2+} and Fe^{3+} in octahedral sites. Co and Zn has bigger radii in octahedral sites more than Fe^{3+} which results in

Table 1. Crystallinity, crystallite size and lattice parameter of $Co_{1-X}Zn_XFe_2O_4$.

Structure	Intensity x Crystallinity (u.a)	Crystallinity index (%)	Crystallite size (nm)	θ	Lattice Parameter
$CoFe_2O_4$	3294.40	36.58	37.33	17.78	8.3729
$Co_{0,8}Zn_{0,2}Fe_2O_4$	5647.07	62.71	43.66	17.74	8.3912
$Co_{0,2}Zn_{0,8}Fe_2O_4$	9004.56	100.00	51.88	17.67	8.4232

increase of lattice constant. Similar behavior is observed for $Co_{0.8}Zn_{0.2}Fe_2O_4$, in which Zn^{2+} and Co^{2+} migrates to octahedral sites. In this case Zn^{2+} migrates completely, replacing the Fe atoms, but a residual Co^{2+} still in tetrahedral sites. It is important note that Co^{2+} in tetrahedral position has a larger radii when compared to Fe^{3+} in tetrahedral and octahedral positions, so the total migration of Zn^{2+} and the partial migration of Co^{2+} to octahedral sites, causes the increment in lattice constant.

The Rietveld method used for the data neutron diffraction of powder consists of a theoretical adjustment calculated from experimentally measured crystallographic information[22]. In the practical part will be used free software MAUD (Materials Analysis Using Diffraction) for the refinement of the diffraction of X-rays.[23-24]. The quality of refinement is available by some indexes, like weighted profile factor R_{wp}. If R_{wp} is decreasing, then the refinement process is successful. "Sig" or "GoF - Goodness of Fit" refers to the standard setting grade used in the experimental XRD patterns results, usually we look for low values for Sig[25]. R_{EXP} is expected weighted profile factor and R_b is the Bragg factor, they are defined like as follows[26]:

$$Sig \ or \ GoF = \frac{R_{WP}}{R_{Exp}} \quad (5)$$

$$R_{WP} = \left[\frac{\Sigma w_i \cdot (I_{io} - I_{ic})^2}{\Sigma w_i \cdot I_{io}^2} \right] \quad (6)$$

$$R_{Exp} = \left[\frac{N - P}{\Sigma w_i \cdot I_{io}^2} \right] \quad (7)$$

$$R_b = \frac{\Sigma |I_{ko} - I_{kc}|}{\Sigma I_{ko}} \quad (8)$$

I_{io} and I_{ic} are the observed and calculated intensities at i_{th} step. I_k represent the intensities assigned to the K_{th} Bragg reflection at the end of the refinement cycles, $W_i = (1/I_{io})$ is the weight factor and (N-P) is the number of degrees of freedom[26]. To evaluate the quality of refinement, the disagreement indexes "Sig" and "R_{wp}"[22] are used, and these parameters must present values less than 2, for materials with two or more phases. For the process to be considered a good refinement "Sig" parameter needs to be closer to one, better will be the process efficiency[22,25,27]. In this work we use Rietveld method to quantify indexes phases to XRD and calculate the lattice parameters. All results by Rietveld Method are summarized in Table 2 and graphs from Maud are in Figures 2; 3 and 4.

Figure 2. $CoFe_2O_4$ sample refinement
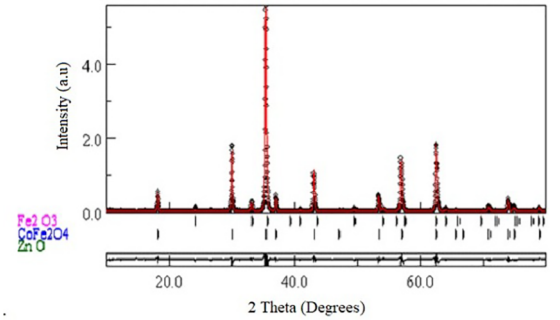
Figure 3. $Co_{0.8}Zn_{0.2}Fe_2O_4$ sample refinement
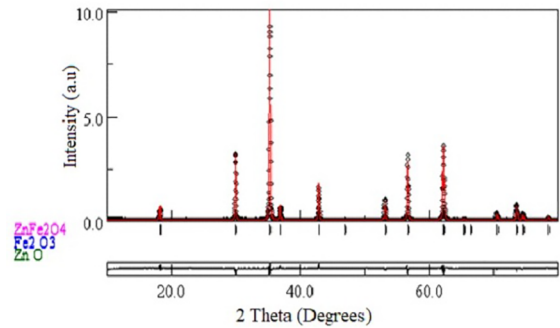
Figure 4. $Co_{0.2}Zn_{0.8}Fe_2O_4$ sample refinement

Rietveld refinement was performed multiple times, searching small values of R's parameters. the refinement was proceeded by several settings in chemical composition of ferrites by changing atoms to octahedral and tetrahedral sites. In Figure 2 we can observe $CoFe_2O_4$ refinement.

Refined parameters R_{WP} (%) 12,3988, R_b (%) 9,2986; Sig 1,2654, and R_{exp} (%) 9,7983, presented a broadening

Table 2. Rietveld parameters of $Co1-XZnXFe_2O_4$

Composition	Sig (GOF)	R_{wp}(%)	R_b(%)	R_{exp}(%)	Phases (%)		a
$CoFe_2O_4$	1.2654	12.3988	9.2986	9.7983	Spinel 92.3775	Fe_2O_3 7.6225	8.3731
$Co_{0.8}Zn_{0.2}Fe_2O_4$	1.5213	13.2595	10.4656	8.7160	Spinel 92.2892	Fe_2O_3 7.7108	8.3930
$Co_{0.2}Zn_{0.8}Fe_2O_4$	1.4044	12.3372	9.3424	8.7849	Spinel 100		8.4248

a = Lattice parameter

Tunable Magnetic and Electrical Properties of Cobalt and Zinc Ferrites $CO_{1-X}Zn_XFe_2O_4$ Synthesized by Combustion Route

5

of the peaks and a decrease in their intensity. By Rietveld we can indexed two phases to $CoFe_2O_4$, one major phase that can be indexed to spinel phase and another that can be indexed to Fe_2O_3. In the absence of zinc element in composition of ferrite, there is an intense occupation of octahedral sites by Co^{2+}, Fe^{2+} and Fe^{3+}. The lattice parameter estimated by Rietveld was close to be determined experimentally (Table 1). The best settings occurs when Fe atoms migrates to tetrahedral positions e Co atoms migrates to octahedral positions, resulting small values of Sig, R_{wp}, R_{exp} and R_b for this adaptation.

In figures 3 and 4 we see the Rietveld refinements by $Co_{0.8}Zn_{0.2}Fe_2O_4$ and $Co_{0.2}Zn_{0.8}Fe_2O_4$. For $Co_{0.8}Zn_{0.2}Fe_2O_4$ we can index the XRD to two major phases, one to spinel phase and another to Fe_2O_3. In the composition $Co_{0.2}Zn_{0.8}Fe_2O_4$ was observed a formation of a single phase index to spinel phase, the low values of Sig, R_{wp}, R_{exp} and R_b were achieved by change in atoms positions replacing atoms of Fe by Zn in B sites, and atoms of Fe will displace Zn and Co in A sites.

In figure 3 is shown the ferrite composition $Co_{0.8}Zn_{0.2}Fe_2O_4$, the refined parameters for this ferrite are $R_{wp(\%)}$ 13,2595; $R_{b(\%)}$ 10,4656; Sig 1,5213 and $R_{exp\,(\%)}$ 8,7160.

In Figure 4 we observe the ferrite $Co_{0.2}Zn_{0.8}Fe_2O_4$ refined composition in R_{wp} parameters (%) 12,3372; R_b (%) 9,3424; Sig 1,4044 and R_{exp} 8,7849 having narrow peaks with high intensity, indicating high material crystallinity with increase of zinc concentration.

3.2 Scanning electron microscopy

Scanning Electron Microscopy (SEM) was performed with magnification of 5000x on 15 kV and resolution of 512 x 384 pixels, with images of 32,3 μm for these compositions. The images show particles with uniform morphology irregular size and high concentration of open pores, indicating that some compositions may present segregation of components with consequent volatilization. Figure 5 (a) shows the scanning electron microscopy of the $CoFe_2O_4$ composition; Figure 5 (b) shows the SEM of $Co_{0.8}Zn_{0.2}Fe_2O_4$ composition and Figure 5 (c) shows the SEM of $Co_{0.2}Zn_{0.8}Fe_2O_4$

The growth of the crystallite size is favored by temperature and ionic diffusion. There is formation of agglomerates due to "intermolecular" interactions of van der Waals type; with spherical morphology of agglomerates composed of cubic structure ferrite nanocrystals, according to results obtained by XRD patterns.

3.3 Cation distribution and magnetic properties

The lattice parameter is sensible to cation distribution in octahedral and tetrahedral sites. In present work we supposed the cation distribution by the following relations[28,29]:

$$a_{th} = \frac{8}{3\sqrt{3}}\left[(r_a + R_0) + \sqrt{3}\,(r_b + R_0)\right] \qquad (9)$$

(a) – SEM of CoFe₂O₄
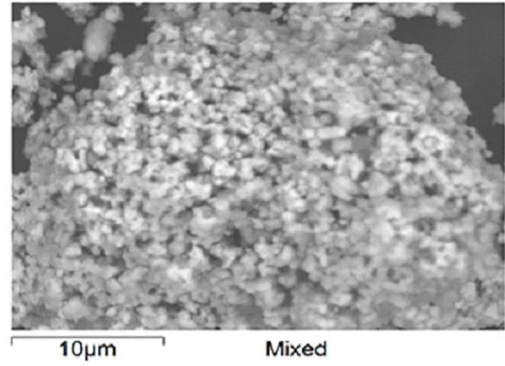
(b) – SEM of Co₀.₈Zn₀.₂Fe₂O₄
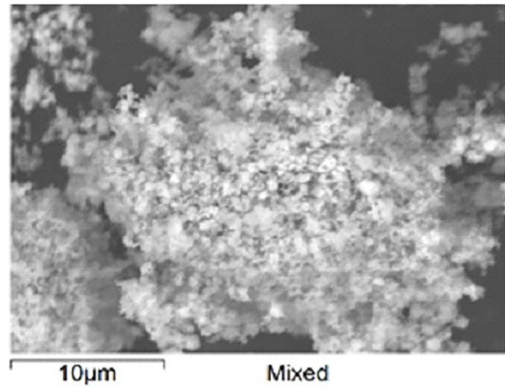
(c) – SEM of Co₀.₂Zn₀.₈Fe₂O₄
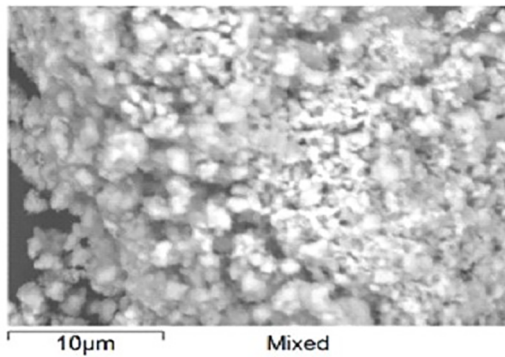
Figure 5. (a) SEM of $CoFe_2O_4$, (b) SEM of $Co_{0.8}Zn_{0.2}Fe_2O_4$ and (c) SEM of $Co_{0.2}Zn_{0.8}Fe_2O_4$

$$r_a = \Sigma a_i \cdot r_i \qquad (10)$$

$$r_b = \frac{1}{2}\Sigma a_i \cdot r_i \qquad (11)$$

In equation 9. a_{th} is theorical lattice parameter, r_a is the average radius on tetrahedral positions, r_b is the average radius on octahedral positions and R_O is the radius of oxygen. The parameters r_a and r_b are shown in equations 10 and 11, on which a_i is ionic concentration of species in tetrahedral and octahedral positions and r_i is the radius of ionic species Zn^{2+}, Co^{2+}, Fe^{2+}, Fe^{3+}. All results are shown on table 3.

We use a_{th} for estimate the cation distribution and from it calculate theoretical Bohr magneton, the experimental Bohr magneton[30-31] was calculated by equation 12.

$$n_B = \frac{M_{wt} \cdot M_s}{5585} \qquad (12)$$

In equation 12. μ_B is theoretical Bohr magneton, M_{wt} is the molecular weight of sample and M_s is the saturation magnetization. We compare experimental Bohr magneton with theoretical Bohr magneton $n_B^{Theo} = M(B) - M(A)$ [32-34], here $M(B)$ is magnetization on site B (octahedral) and $M(A)$ is magnetization on site A (tetrahedral). In our study we have the following elements: Fe^{3+} (5 μ_B), Fe^{2+} (4 μ_B), Co^{2+} (3 μ_B) and Zn^{2+} (0 μ_B), each ionic species has its magnetic moment estimated by bohr magneton coming from eletronic distribution on d orbital. By Néel's theory, the resulting magnetization is supported through the difference between magnetization on B site by A site, and both sites are collinear and antiparallel each other.

In table 3 is possible observe that with the Zn^{2+} increment the μ_b decreases, for a good agreement between μ_B and $\mu_B^{(Theo)}$, we admit that all ionic species can migrate for both sites. For $CoFe_2O_4$ the best matchup is when most of Fe^{3+} (5 μ_B) and a smaller part of Fe^{2+} (4 μ_B) migrates from B site to A site, and Co^{2+} (3 μ_B) originally in A site go to B site. This migration decreases the experimental and theoretical Bohr magneton. For $Co_{0.8}Zn_{0.2}Fe_2O_4$ and $Co_{0.2}Zn_{0.8}Fe_2O_4$, there is a presence of a non magnetic ion Zn^{2+} (0 μ_B). The best concordance occurs when Zn^{2+} and Co^{2+} goes to octahedral site, so the net magnetic moment decreases with the increase of Zn^{2+} and Co^{2+} in B site. The presence of Co^{2+} and Zn^{2+} causes a decrease in magnetization of B site, while ions with large magnetic moments will be in A site, which will lead to an increase in magnetization on site A, so the difference between them will be smaller, justifying the fact that the higher the increase of Zn, the smaller the magnetization.

VSM graphs and hysteresis loops of $Co_{1-x}Zn_xFe_2O_4$ are shown in figure 6, magnetic properties like M_s (saturation magnetization), H_C (coercivity Field), M_R (remanent Magnetization), squareness ratio and anisotropy crystallinity were calculated and all results for VSM analysis at room temperature are summarized in table 4
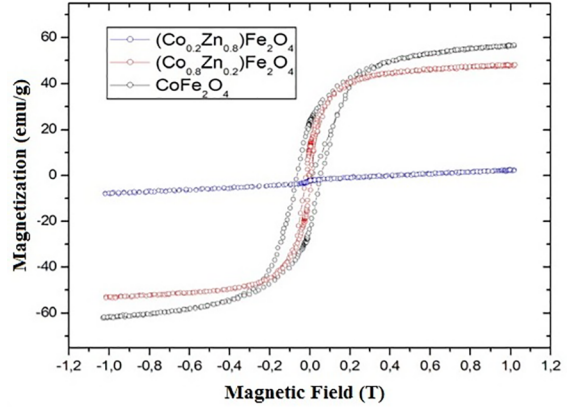
Figure 6. Magnetic hysteresis of $Co_{1-X}Zn_XFe_2O_4$

The saturation magnetization found in this work decreases significantly with the addition of Zn^{2+}. For $CoFe_2O_4$, $Co_{0.8}Zn_{0.2}Fe_2O_4$ and $Co_{0.2}Zn_{0.8}Fe_2O_4$ the M_S decreases from 56.72, 47.98 and 2.50 emu/g, respectively. Basically the Zn^{2+} and Co^{2+} replaces the Fe^{2+} and Fe^{3+} in octahedral sites, forcing a migration of Fe^{2+} and Fe^{3+} to tetrahedral sites, decreasing the magnetic moment of $CoFe_2O_4$. H_R and H_C were found with a reduction to 22,64 Oe to 0 Oe and 500 G to 0 G respectively, with the increase of zinc concentration.

In this work we use coercivity and saturation magnetization to determine the anisotropy constant (K)[30,35], using the following relationship:

$$H_c = \frac{0.96 \cdot K}{M_s} \qquad (13)$$

Table 3. Proposed cation distribution for $Co_{1-x}Zn_xFe_2O_4$.

Sample	Site A	Site B	Lattice Parameter	$n_{b(The)}$	$n_{b(Exp)}$
$CoFe_2O_4$	$Fe_{0.85}^{3+}Fe_{0.15}^{2+}$	$Fe_{0.7}^{3+}Fe_{0.2}^{2+}Co_1^{2+}$	8,3725	2,45	2.38
$Co_{0.8}Zn_{0.2}Fe_2O_4$	$Fe_{0.88}^{3+}Fe_{0.12}^{2+}$	$Co_{0.8}^{2+}Zn_{0.2}^{2+}Fe_{0.88}^{3+}Fe_{0.12}^{2+}$	8,3909	2,4	2.03
$Co_{0.2}Zn_{0.8}Fe_2O_4$	$Co_{0.05}^{2+}Fe_{0.7}^{3+}Fe_{0.25}^{2+}$	$Co_{0.15}^{2+}Zn_{0.8}^{2+}Fe_{0.55}^{3+}Fe_{0.5}^{2+}$	8,4250	0,55	0.11

$n_{b(theo)}$ = Bohr magneton theorical

Table 4. Magnetic properties of $Co_{1-X}Zn_XFe_2O_4$.

Ferrite	M_s (emu/g)	M_R (emu/g)	M_R/M_s	H_C (Tesla)	H_C (Gauss/Oe)	K (erg/g) x10^3
$CoFe_2O_4$	56.72	22.64	0.40	0,05	500	29,54
$Co_{0.8}Zn_{0.2}Fe_2O_4$	47.98	12.62	0.26	0,025	250	12,49
$Co_{0.2}Zn_{0.8}Fe_2O_4$	2.50	0.00	0.00	0	0.00	0.00

M_s = Saturation magnetization; M_R = Remanent magnetization; H_C = coercivity field; K=Anisotropy constant; M_R/M_s = Squareness

Tunable Magnetic and Electrical Properties of Cobalt and Zinc Ferrites CO$_{1-X}$Zn$_X$Fe$_2$O$_4$ Synthesized by Combustion Route

7

CoFe$_2$O$_4$ has the largest anisotropy constant while with the increase of Zn^{2+} the constant reduces, and Co$_{0.2}$Zn$_{0.8}$Fe$_2$O$_4$ has the smaller anisotropy constant. This effect is visible in high zinc concentrations. In this case H$_C$ and H$_R$ reach the lowest values. The decrease in anisotropy constant indicates that dipoles of magnetic moments has a strong dependence in a given direction. Squareness was calculated by all samples and are shown in table 3.5. If Mr/Ms is equal or higher than 0,5 this material is considered in a single magnetic domain. If squareness is smaller than 0,5, material synthesized has a multi domain structure[35,36]. All ferrites in this work are multi domain type.

Co$_{0.2}$Zn$_{0.8}$Fe$_2$O$_4$ has a behavior of paramagnetic material, as noted by the hysteresis curve, almost linear, and with a small saturation of magnetization and with a small coercitivity, showing up as a magnetically soft material, which has possibilities of applications in antennas and other devices in wireless communication systems, especially in the microwave region[37,38]. Co$_{0.8}$Zn$_{0.2}$Fe$_2$O$_4$ has high magnetization and low hysteresis loss of energy. However, CoFe$_2$O$_4$ has a characteristic behavior of a hard magnetic material, presenting a wide hysteresis, such materials are characteristic to have a permanent field, difficult to demagnetize and believed to have potential for a wide range of engineering applications, such as drug delivery, bioseparation and magnetic resonance imaging [16,39,40].

3.4 Electrical properties

The following electrical properties of ferrites are shown in Figure 7: (a): permittivity and (b) loss tangent. These properties were determined using a network analyzer at frequency range of 8,0 GHz to 12,5 GHz. This information is important for materials intended to be applied in telecommunications technology. The curves presents low permittivity, with a mean value of 1.0 as function of the frequency applied, indicating its functionality possibilities to work with terahertz frequency. Others have larger electrical permittivity values, with range of 4-5 for high frequency bands which have been applied. However these ceramic materials have small loss tangent levels. Because of the complementarities between magnetic loss and dielectric loss can induce the ferrites Co$_{0.8}$Zn$_{0.2}$Fe$_2$O$_4$ and CoFe$_2$O$_4$ to have excellent properties for absorption in the microwave range[41,42].

Figures 7 (a) and 7 (b) shows the results of permittivity and loss tangent in the frequency range of 8,0 GHz to 12,5 GHz, all measurements were realized in vector network analyzer ROHDE & SCHWARZ. It was concluded that a higher amount of zinc in the sample and the migration of Zinc to octahedral sites, you can get lower permittivity without major changes in the electrical losses of the material.

Ferrites presenting thinner hysteresis (soft material) as the Co$_{0.8}$Zn$_{0.2}$Fe$_2$O$_4$ composition, has magnetic permeability that is characteristic of ferromagnetic materials with high electrical permittivity, low resistivity, and low residual field, enabling applications in various technological areas such as automotive, telecommunications, electrical, electronics, etc. The physical properties of these materials indicate that their magnetization states can be abruptly changed with a relatively small variation in field intensity. The Ferrite sample in Co$_{0.2}$Zn$_{0.8}$Fe$_2$O$_4$ composition is presented as a material with antiferromagnetic properties of very low electrical permittivity and low electrical loss tangent. Materials with these characteristics have magnetic susceptibility value less than zero. Applications of materials with these features are used in devices that require antennas with receiving technology, which is needed to operate at high frequencies of terahertz order, due to their very low electrical permittivity as well in the use of devices of dielectric antenna technology (DRA) as being an excellent option. The toroidal cores of switched-mode power supply transformers uses ferrites materials with these characteristics[37-39]. These materials have characteristics which allows their use both as insaturable reactors, and in switched-mode power supply transformers, with high dielectric constant and low loss rate, making them potential candidates for microwave and dielectric resonators[40-42].
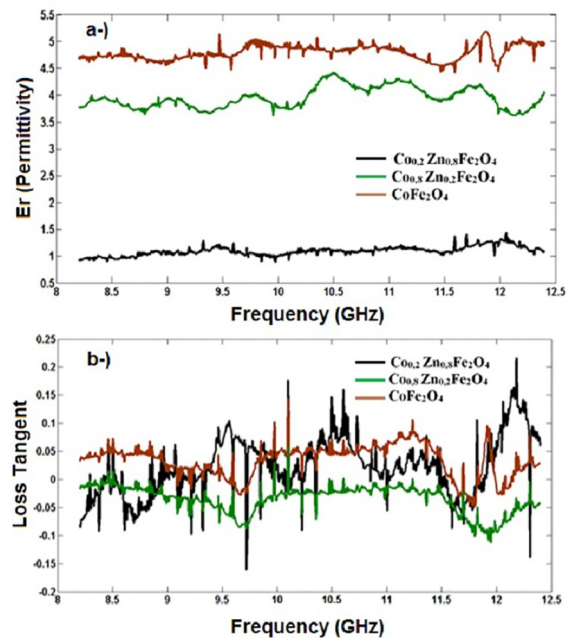
Figure 7. (a) Electrical permittivity versus frequency in GHz; (b) Loss Tangent versus frequency of Co$_{1-X}$Zn$_X$Fe$_2$O$_4$

The ferrite sample obtained in this work with the CoFe$_2$O$_4$ composition in which curve has larger hysteresis,

namely wider (hard material), has characteristics peculiar to a material that can be used in saturable reactors, electric motors, instruments for measuring electric quantities and acoustic transducers such as microphones and speakers[43-45].

The sample that showed best simultaneous results was $Co_{0.2}Zn_{0.8}Fe_2O_4$. It has low saturation magnetization and remaining magnetization, smalls coercive field and hysteresis loss. In addition $Co_{0.2}Zn_{0.8}Fe_2O_4$ also exhibits low electrical permittivity and small loss tangent, it is shown that its magnetic and electrical properties are interesting to applications in telecommunications devices.

4. Conclusions

$Co_{(1-X)}Zn_{(X)}Fe_2O_4$ (where x = 0,0; 0,2; 0,8) samples have been successfully synthesized via chemical combustion reaction method. XRD results confirmed that with the increase of Zn^{2+}, the lattice parameter and crystallite size also increases. Cation distribution shows the preference of Zn^{2+} for B sites. It was clearly noticeable that the variation of the concentration of the cobalt element and the introduction of the element Zn exerted a predominant influence on the magnetic behavior of the ferrite samples prepared in this work. Briefly, in terms of magnetic properties, it was found that the obtained sample containing 0,2 mol of Zn was presented as a soft material, with changes in saturation magnetization and coercivity field when compared to the sample containing zero concentration of Zn presented as a hard material. This difference in the hysteresis of these both samples will inevitably imply differences in their magnetic behavior potentials. Possible applications of these ceramic powders ferrite obtained in this study are in the industrial or electronics market, which are of great importance due to their low cost and easy production through simpler synthesis methods, such as combustion reaction.

5. Acknowledgements

6. References

1. Banerjee A, Bid S, Dutta H, Chaudhuri S, Das D, Pradhan SK. Microstructural changes and effect of variation of lattice strain on positron annihilation lifetime parameters of zinc ferrite nanocomposites prepared by high enegy ball-milling. *Materials Research*. 2012;15(6):1022-1028.

2. Alves TEP, Pessoni HVS, Franco A Jr. The effect of Y^{3+} substitution on the structural, optical band-gap, and magnetic properties of cobalt ferrite nanoparticles. *Physical Chemistry Chemical Physics*. 2017;19(25):16395-16405.

3. Fernandes C, Pereira C, Fernández-García MP, Pereira AM, Guedes A, Fernández-Pacheco R, et al. Tailored design of $Co_xMn_{1-x}Fe_2O_4$ nanoferrites: a new route for dual control of size and magnetic properties. *Journal of Materials Chemistry C*. 2014;2(29):5818-5828.

4. Kumar H, Singh JP, Srisvastava RC, Negi P, Agrawal HM, Asokan K. FTIR and Electrical Study of Dysprosium Doped Cobalt Ferrites Nanoparticles. *Journal of Nanoscience*. 2014;2014:862415.

5. Sabikoğlu İ, Parali L, Malina O, Novak P, Kaslik J, Tucek J, et al. The effect of neodymium substitution on the structural and magnetic properties of nickel ferrite. *Progress in Natural Science: Materials International*. 2015;25(3):215-221.

6. Abdulmajeed IM, Khalil LS. Structural and Optical Properties of $Co_{1-x}Zn_xFe_2O_4$ Synthesis by Sol-Gel Auto Combustion Method. *International Journal of Current Engineering and Technology*. 2016;6(3):976-981.

7. Jamil MT, Ahmad J, Bukhari SH, Sultan T, Akhter MY, Ahmad H, et al. Effect on structural and optical properties of Zn-substituted cobalt ferrite $CoFe_2O_4$. *Journal of Ovonic Research*. 2017;13(1):45-53.

8. Sun GL, Li JB, Sun JJ, Yang XZ. The influences of Zn^{2+} and some rare-earth ions on the magnetic properties of nickel-zinc ferrites. *Journal of Magnetism and Magnetic Materials*. 2004;281(2-3):173-177.

9. Munir A, Ahmed F, Saqib M, Anis-ur-Rehman M. Electrical Properties of Ni-Zn Ferrite Nanoparticles Prepared by Simplified Sol-Gel Method. *Journal of Superconductivity and Novel Magnetism*. 2014;28(3):983-987.

10. Zhang Y, Xia A, Chen W, Ma R. Structural and Magnetic Properties of Hydrothermal Spinel $Ni_{0.4}Zn_{0.6}Fe_2O_4$ Ferrites. *Materials Research*. 2015;18(6):1251-1255.

11. Gharagozlou M, Bayati R. Low temperature processing and magnetic properties of zinc ferrite nanoparticles. *Superlattices and Microstructures*. 2015;78:190-200.

12. Kakade SG, Kambale RC, Kolekar YD, Ramana CV. Dielectric, electrical transport and magnetic properties of Er^{3+} substituted nanocrystalline cobalt ferrite. *Journal of Physics and Chemistry of Solids*. 2016;98:20-27.

13. Sharma S, Sharma ND, Choudhary N, Verma MK, Singh D. Chromium incorporated nanocrystalline cobalt ferrite synthesized by combustion method: Effect of fuel and temperature. *Ceramics International*. 2017;43(16):13401-13410.

14. Deshmukh SS, Humbe AV, Kumar A, Dorik RG, Jadhav KM. Urea assisted synthesis of $Ni_{1-X}Zn_xFe_2O_4$ ($0 \le x \le 0.8$): Magnetic and Mössbauer investigations. *Journal of Alloys and Compounds*. 2017;704:227-236.

15. Mukasyan AS, Epstein P, Dinka P. Solution combustion synthesis of nanomaterials. *Proceedings of the Combustion Institute*. 2007;31(2):1789-1795.

16. Slatineanu T, Iordan AR, Oancea V, Palamaru MN, Dumitru I, Constantin CP, Caltun OF.. Magnetic and dielectric properties of Co-Zn ferrite. *Materials Science and Engineering: B*. 2013;178(16):1040-1047.

Tunable Magnetic and Electrical Properties of Cobalt and Zinc Ferrites CO$_{1-X}$Zn$_X$Fe$_2$O$_4$ Synthesized by Combustion Route

9

17. Jain SR, Adiga KCA, Verneker VRP. A new approach to thermochemical calculations of condensed fuel-oxidizer mixture. *Combustion and Flame*. 1981;40:71-79.

18. Miranda EAC, Carvajal JFM, Baena OJR. Effect of the Fuels Glycine, Urea and Citric Acid on Synthesis of the Ceramic Pigment ZnCr$_2$O$_4$ by Solution Combustion. *Materials Research*. 2015;18(5):1038-1043.

19. Thakur P, Sharma R, Sharma V, Barman PB, Kumar M, Barman D, et al. Gd^{3+}doped Mn-Zn soft ferrite nanoparticles: Superparamagnetism and its correlation with other physical properties. *Journal of Magnetism and Magnetic Materials*. 2017;432:208-217.

20. Ben Ali M, El Maalam K, El Moussaoui H, Mounkachi O, Hamedoun M, Masrour R, et al. Effect of zinc concentration on the structural and magnetic properties of mixed Co-Zn ferrites nanoparticles synthesized by sol/gel method. *Journal of Magnetism and Magnetic Materials*. 2016;398:20-25.

21. A.S. Group. *Database of Ionic Radii*; 1976. Available from: <http://abulafia.mt.ic.ac.uk/shannon/ptable.php>. Access in: 17/11/2017.

22. Rietveld HM. A Profile Refinement Method for Nuclear and Magnetic Structures. *Journal of Applied Crystallography*. 1969;2:65-71.

23. Lutterotti L. Quantitative Rietveld analysis in batch mode with Maud. *IUCR CPD Newsletter*. 2005;32:53-55.

24. Lutterotti L. *MAUD software*. Version 2.26 ; 2011. Available from: http://www.ing.unitn.it/~maud>. Access in: 20/01/2017.

25. Rietveld HM. Line profiles of neutron powder-diffraction peaks for structure refinement. *Acta Crystallographica*. 1967;27:151-152.

26. Dalal M, Mallick A, Mahapatra AS, Mitra A, Das A, Das D, et al. Effect of cation distribution on the magnetic and hyperfine behaviour of nanocrystalline Co doped Ni-Zn ferrite (Ni$_{0.4}$Zn$_{0.4}$Co$_{0.2}$Fe$_2$O$_4$). *Materials Research Bulletin*. 2016;76:389-401.

27. Pitschke W, Mattern N, Hermann H. Incorporation of microabsorption corrections into Rietveld analysis. *Powder Diffraction*. 1993;8(4):223-228.

28. Sharifi I, Shokrollahi H, Doroodmand MM, Safi R. Magnetic and structural studies on CoFe$_2$O$_4$ nanoparticles synthesized by co-precipitation, normal micelles and reverse micelles methods. *Journal of Magnetism and Magnetic Materials*. 2012;324(10):1854-1861.

29. Karimi S, Kameli P, Ahmadvand H, Salamati H. Effects of Zn-Cr-substitution on the structural and magnetic properties of Ni$_{1-x}$Zn$_x$Fe$_{2-x}$Cr$_x$O$_4$ ferrites. *Ceramics International*. 2016;42(15):16948-16955.

30. Tatarchuk TR, Paliychuk ND, Bououdina M, Al-Najar B, Pacia M, Macyk W, et al. Effect of cobalt substitution on structural, elastic, magnetic and optical properties of zinc ferrite nanoparticles. *Journal of Alloys and Compounds*. 2018;731:1256-1266.

31. Chen W, Liu D, Wu W, Zhang H, Wu J. Structure and magnetic properties evolution of rod-like Co$_{0.5}$Ni$_{0.25}$Zn$_{0.25}$Dy$_X$Fe$_{2-X}$O$_4$ synthesized by solvothermal method. *Journal of Magnetism and Magnetic Materials*. 2017;422: 49-56.

32. Kumar L, Kumar P, Kar M. Cation distribution by Rietveld technique and magnetocrystalline anisotropy of Zn substituted nanocrystalline cobalt ferrite. *Journal of Alloys and Compounds*. 2013;551:72-81.

33. Nikmanesh H, Kameli P, Asgarian SM, Karimi S, Moradi M, Kargar Z, et al. Positron annihilation lifetime, cation distribution and magnetic features of Ni$_{1-x}$Zn$_x$Fe$_{2-x}$Co$_x$O$_4$ ferrite nanoparticles. *RSC Advances*. 2017;7(36):22320-22328.

34. Heiba ZK, Mohamed MB, Wahba AM, Arda L. Magnetic and Structural Properties of Nanocrystalline Cobalt-Substituted Magnesium-Manganese Ferrite. *Journal of Superconductivity and Novel Magnetism*. 2015;28(8):2517-2524.

35. Saffari F, Kameli P, Rahimi M, Ahmadvand H, Salamati H. Effects of Co-substitution on the structural and magnetic properties of NiCo$_x$Fe$_{2-x}$O$_4$ ferrite nanoparticles. *Ceramics International*. 2015;45(6):7352-7358.

36. Ateia EE, Soliman FS. Modification of Co/Cu nanoferrites properties via Gd^{3+}/Er^{3+}doping. *Applied Physics A: Materials Science and Processing*. 2017;123(5):312.

37. Mohamed MB, El-Sayed KJ. Structure and Microstructure in Relation to Magnetic/Dielectric Properties of Nanocrystalline Ni$_{1-x}$Zn$_x$Fe$_{1.5}$Cr$_{0.5}$O$_4$ Ferrite. *Journal of Superconductivity and Novel Magnetism*. 2015;28(7):2121-2131.

38. Lin CC, Ho JM, Wu MS. Continuous preparations of Fe$_3$O$_4$ nanoparticles using a rotating packed bed: Dependence of size and magnetic property on temperature. *Powder Technology*. 2015;274:441-445.

39. Raut AV, Barkule RS, Shengule DR, Jadhav KM. Synthesis, structural investigation and magnetic properties of Zn^{2+} substituted cobalt ferrite nanoparticles prepared by the sol-gel auto-combustion technique. *Journal of Magnetism and Magnetic Materials*. 2014;358-359:87-92.

40. Manikandan A, Durka M, Antony SA. A Novel Synthesis, Structural, Morphological, and Opto-magnetic Characterizations of Magnetically Separable Spinel Co$_x$Mn$_{1-X}$ Fe$_2$O$_4$ ($0 \leq x \leq 1$) Nano-catalysts. *Journal of Superconductivity and Novel Magnetism*. 2014;27:2841-2857.

41. Liu P, Huang Y, Zhang X. Preparation and excellent microwave absorption properties of ferromagnetic graphene/poly (3,4-ethylenedioxythiophene)/CoFe$_2$O$_4$ nanocomposites. *Powder Technology*. 2015;276:112-117.

42. Hidaka M, Tokiwa N, Fujii M, Watanabe S, Akimitsu J. Correlation between the structural and antiferromagnetic phase transitions in ZnCr$_2$Se$_4$. *Physica Status Solidi b*. 2003;236(1):9-18.

43. Druc AC, Borhan AI, Diaconu A, Iordan AR, Nedelcu GG, Leontie L, et al. How cobalt ions substitution changes the structure and dielectric properties of magnesium ferrite? *Ceramics International*. 2014;40(8 Pt B):13573-13578.

44. Yang H, Ye T, Lin Y, Zhu J, Wang F. Microwave absorbing properties of the ferrite composites based on graphene. *Journal of Alloys and Compounds*. 2016;683:567-574.

45. Zheng Y, Wang S, Feng J, Li C, Ouyang Z, Liu J, et al. Regulation mechanism of EM parameters in natural ferrite and its application in microwave absorbing materials. *Science in China Series E*. 2006;49(1):38-49.